

# Localized surface plasmon resonance coupling in Au nanoparticles/phosphorus dendrimer multilayer thin films fabricated by layer-by-layer self-assembly method†

Wen Bo Zhao,<sup>a</sup> Jeongju Park,<sup>b</sup> Anne-Marie Caminade,<sup>c</sup> Seong-Jun Jeong,<sup>d</sup> Yoon Hee Jang,<sup>a</sup> Sang Ouk Kim,<sup>d</sup> Jean-Pierre Majoral,<sup>c</sup> Jinhan Cho<sup>\*b</sup> and Dong Ha Kim<sup>\*a</sup>

Received 14th August 2008, Accepted 5th January 2009

First published as an Advance Article on the web 11th February 2009

DOI: 10.1039/b814116a

Multilayer thin films of anionic gold nanoparticles (Au<sub>NPs</sub>) and cationic phosphorus dendrimers were deposited on 3-(diethoxymethyl-silyl)propylamine (3-APDMES)-coated substrates using layer-by-layer (LbL) assembly driven by electrostatic interactions. The growth of Au/dendrimer multilayers composed of Au<sub>NPs</sub> with diameters of ~3 nm and ~16 nm and dendrimer with ~2 nm diameter was monitored by UV-vis spectroscopy. The relative amounts of Au<sub>NPs</sub> and dendrimers in the multilayer films were calculated using a quartz crystal microbalance. The Au-containing multilayers have two surface plasmon bands at ~530 nm and ~600 nm, where the latter exhibits a red shift upon increasing the areal density of AuNPs as well as increasing the layer number. The localized surface plasmon resonance (LSPR) band of the hybrid films can be tuned by adding NaCl to the dendrimer solution or by removing the organic matrix. These results demonstrate that the near-field coupling between the LSPR bands of neighboring Au layers is responsible for the controlled absorption behavior. Au mesoporous films after removing dendrimers show LSPR sensing properties for alcohols with different refractive indices in the range 1.33–1.41. A linear relationship was obtained between the LSPR peak wavelength and the refractive index of the surrounding medium.

## Introduction

Hybrid nanostructures containing two or more components with different functionalities with controlled structure and interface interactions are attractive candidates for advanced applications. With different dimensions and material parameters integrated from individual components, the properties and applications of the constituent components can be optimized independently. Such multicomponent systems may even achieve entirely new properties *via* synergistic coupling between the constituent species.<sup>1</sup> Studies on hybrid nanomaterials with noble metal nanoparticles are especially important because these materials have potential as elements in biosensor,<sup>2</sup> molecular diagnostics,<sup>3</sup> optoelectronics,<sup>4</sup> magnetic and catalytic<sup>1,5</sup> devices. Gold nanoparticles (Au<sub>NPs</sub>) have been exploited in a variety of applications

based on their unique optical and electronic properties. These properties are obtained mainly due to the localized surface plasmon resonance (LSPR) absorption in the visible region.<sup>6</sup> The LSPR is a collective oscillation of the nanoparticle's conduction electrons in nanoparticles when they are excited by incident electromagnetic radiation at a specific wavelength. The LSPR band of a noble metal nano-objects relies on its size, shape, composition and its surrounding medium.<sup>7</sup>

In addition to these primary factors, increasing attention has been paid to the role of coupling between surface plasmons of neighboring noble metal objects. Recently many pioneering theoretical and experimental works on coupling behavior have been reported.<sup>8</sup> Ghosh and Pal summarized in a substantial review the varieties of synthetic strategies and characterization of nanoscale Au<sub>NPs</sub> assembled into an aggregate structure, and exploration of the optical properties of Au nanoparticles in a close-packed assembly.<sup>8a</sup> El-Sayed *et al.* investigated LSPR of dimer and trimer of Au spheres and of more complex nanostructured geometries using microabsorption spectroscopy and electrodynamic simulations.<sup>8b,c</sup> The fractional plasmon wavelength shift for polarization along the interparticle axis decays nearly exponentially with the interparticle gap. They have also shown how the particle shape, elongation, and curvature influence the coupling-induced plasmon shift without affecting the universal size-scaling behavior. Schatz and Van Duyne studied the electromagnetic interactions between noble metal nanoparticles by measuring the extinction spectra of two-dimensional arrays of Au and Ag cylinders and trigonal prisms that were fabricated with electron beam lithography.<sup>8d,e</sup> Blue shifts of the

<sup>a</sup>Department of Chemistry and Nano Science, Ewha Womans University, 11-1 Daehyun-Dong, Seodaemun-Gu, Seoul, 120-750, Korea. E-mail: dhkim@ewha.ac.kr; Fax: +82-2-3277-3419; Tel: +82-2-3277-4517

<sup>b</sup>School of Advanced Materials Engineering, Kookmin University, Chungneung-Dong/Songbuk-Gu/Seoul, 136-702, Korea. E-mail: jinhan@kookmin.ac.kr; Fax: +82-2-910-4320; Tel: +82-2-910-4287

<sup>c</sup>Laboratoire de Chimie de Coordination, CNRS UPR 8241, 205 Route de Narbonne, 31077 Toulouse Cedex 04, France

<sup>d</sup>Department of Materials Science and Engineering, KAIST Institute for the Nanocentury, KAIST, Daejeon, 305-701, Korea

† Electronic supplementary information (ESI) available: UV-vis spectra of Au<sub>NPs</sub> and dendrimer in aqueous solution; FESEM images of Au/G<sub>4</sub>(NH<sup>+</sup>Et<sub>2</sub>Cl<sup>-</sup>)<sub>96</sub> multilayer films prepared under different conditions; QCM data of a [Au<sub>NP</sub>/G<sub>4</sub>(NH<sup>+</sup>Et<sub>2</sub>Cl<sup>-</sup>)<sub>96</sub>]<sub>5</sub> multilayer film before and after UV light irradiation. See DOI: 10.1039/b814116a

maximum extinction spectra are observed for nanoparticle arrays with relatively large lattice spacings (approximately half the LSPR wavelength) for which radiative dipole interactions between the nanoparticles play an important role and retardation effects are large. For smaller lattice spacings (<100 nm), one expects red shifts (for the case in which the electric polarization is in the plane of the array), as lattice spacing is reduced. Rao's group has investigated effects of the interparticle separation on the surface plasmon bands of Au<sub>NPs</sub> films by examining the interaction between alkanethiols and Au<sub>NPs</sub>. Adsorption of alkanethiols causes blue-shifts of the surface plasmon adsorption band, with the magnitude of the shift being proportional to the chain length.<sup>8f</sup>

As an alternative approach to utilize versatile functions of Au<sub>NPs</sub>, hybrid multilayer thin films containing Au<sub>NPs</sub> fabricated by layer-by-layer (LbL) assembly have been employed for sensing applications or to tune their optical properties.<sup>9</sup> Recently, it was reported that the unique interactions between Au<sub>NPs</sub> stabilized by 4-(dimethylamino)pyridine and various polyelectrolytes (PEs) could effectively produce LbL assembled multilayer films with tailored optical properties.<sup>9a</sup> Advincula *et al.* investigated the SPR response under different pH conditions for hybrid polyelectrolyte/Au<sub>NPs</sub> films using attenuated total reflection geometry.<sup>9b</sup> Kotov and Liz-Marzan reported that a new band developed as the number of bilayers increased in LbL multilayers containing mixed spherical/triangular/hexagonal Au<sub>NPs</sub>.<sup>9c</sup> Sensitive detection of DNA hybridization using catalytic growth of Au<sub>NPs</sub> enhanced SPR was also demonstrated using LbL assembly films of (PAH/PSS).<sup>9d</sup> Other researchers explored versatile functions of LbL multilayer films of Au<sub>NPs</sub> as nanoreactors, coatings which are responsive to stimuli, substrates for surface-assisted laser desorption/ionization mass spectrometry of peptides and environmental pollutants.<sup>9e-g</sup> Such ultrathin films were endowed with potential applications in the areas of advanced microelectronic devices, electrochemical sensor and bioanalysis. However, a systematic analysis on the coupling phenomena inherent in such hybrid Au-containing multilayer films along with their role as refractive index sensors have not been elucidated yet.<sup>9h</sup>

In this paper, we present a LbL assembly route to construct multilayer thin films of anionic Au<sub>NPs</sub> and cationic phosphorus dendrimers which are deposited on 3-(diethoxymethyl-silyl)propylamine (3-APDMES)-coated substrates based on electrostatic interactions and explore the cooperative function between neighboring Au<sub>NPs</sub> within multilayer films. The adsorbed amounts of Au<sub>NPs</sub> and dendrimers are quantitatively examined using quartz crystal microgravimetry (QCM) measurements. We investigate the LSPR absorption behavior of the Au<sub>NPs</sub>/dendrimer multilayer films by UV-vis spectroscopy. The multilayers typically have two plasmon bands at ~530 nm and ~600 nm, the latter of which exhibits a red-shift with increasing bilayer number. We also demonstrate that LSPR of the films can be tuned by either increasing or decreasing the average distance between neighboring Au<sub>NPs</sub> layers, separated by dendrimer layers, with the addition of salt into the dendrimer solution or the removal of dendrimer layers. Finally, we show the potential application of the resulting mesoporous Au<sub>NPs</sub> films in terms of LSPR sensing of the surrounding alcohol media with different refractive indices.

## Experimental

### Materials

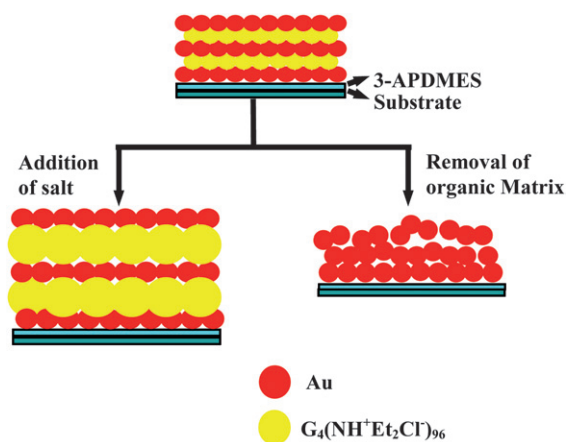
3-APDMES (97%) was purchased from Sigma-Aldrich Company. Au<sub>NPs</sub> with anionic carboxyl functional groups were synthesized according to the literature reported previously.<sup>10</sup> The size of Au<sub>NPs</sub> was ~16 nm or ~3 nm determined by transmission electron microscopy (TEM) (see ESI†). The cationic dendrimers used in this study, denoted G<sub>4</sub>(NH<sup>+</sup>Et<sub>2</sub>Cl<sup>-</sup>)<sub>96</sub>, were N,N-disubstituted hydrazine phosphorus-containing dendrimers of the 4th generation having 96 functional groups on the surface with cationic character.<sup>11</sup> The dendrimer solution was prepared by dissolving it in deionized water at a concentration of 1 mg/ml. The pH value was adjusted to 3–5 using 0.1M hydrochloric acid solution. In order to explore the effect of salt, 0.5 M NaCl was added to the dendrimer solution. The Si and quartz substrates were cleaned in a series of ultrasonically agitated solvents (acetone, ethanol, water) for 15 min, then in a 2.0 (vol%) Hellmanex solution for 15 min at room temperature. In between each sonication step, the substrates were thoroughly rinsed in deionized water several times, and blown dry with nitrogen gas. Water from a Millipore purification system with a resistivity greater than 18.2 MΩ cm was used for deposition and rinsing solutions in all experiments. Methanol, ethanol, 1-propanol, 1-butanol and 1-pentanol were selected as model alcohols and purchased from a local company.

### Fabrication of multilayer films

Clean substrates were placed in a closed glass vessel with 3-APDMES and heated to about 120–140 °C for 3h. After reaction, the substrates were allowed to cool, ultrasonicated in ethanol for a few minutes, rinsed in ethanol and water and then stored for the adsorption experiments. The multilayer assembly was performed on the silanized substrates. First, a substrate was immersed into the Au solution for 10 min (30 min for Au with 3 nm) after which a rinsing step was performed to remove any physically adsorbed molecules, and then blown dry with nitrogen gas. Subsequently, it was immersed into the dendrimer solution for 30 min for assembling the second layer followed by washing and drying in the same manner. This process was repeated until the desired number of layers was deposited. To get the Au nanoporous structure, the samples were subjected to deep UV illumination (λ = 254nm) for 24 hours.

### Characterization

UV-vis spectra were obtained with a S-3100 PDA (SCINCO, Korea) UV-vis spectrophotometer after assembly of each layer on a quartz slide. For QCM measurements, a commercial device (Model: QCM200, SRS) was used to investigate the mass of material deposited after each adsorption step. First, for the deposition of Au<sub>NPs</sub> onto QCM electrodes, cationic poly(allylamine hydrochloride) (PAH) was coated onto the QCM. The resonance frequency of the QCM electrodes was *ca.* 5 MHz. The adsorbed mass of dendrimer and Au<sub>NPs</sub>, Δ*m*, can be calculated from the change in QCM frequency, Δ*F*, according to the Sauerbrey equation:<sup>12</sup> Δ*F* (Hz) = -56.6 × Δ*m*<sub>A</sub>, where Δ*m*<sub>A</sub> is the mass change per quartz crystal unit area, in μg cm<sup>-2</sup>.



**Scheme 1** Schematic diagram of the processes involved in the fabrication of the immobilized colloidal Au<sub>NP</sub> and dendrimer multilayers on a substrate.

## Results and discussion

### Fabrication of hybrid Au/dendrimer multilayer films

The overall procedure to fabricate and modify multilayer films used in this study is illustrated in Scheme 1. The substrates modified with 3-APDMES provide a positively charged surface for adsorption of anionic Au<sub>NPs</sub> with an average size of 3 nm and 16 nm. For comparison, the Au colloidal solution has typical SPR absorption bands at 510.4 nm (for 3 nm-sized Au<sub>NPs</sub>) and 524.6 nm (for 16 nm-sized Au<sub>NPs</sub>). The pH value of the dendrimer solution was adjusted to about 4 for the formation of cationic amine groups. The dendrimer has a characteristic absorption at about 285 nm due to the  $\pi$ - $\pi^*$  transition of the phenyl ring and this absorption peak is overlapped with that of Au<sub>NP</sub> (see ESI,† Fig. S1).

Fig. 1 shows the change in UV-visible extinction spectra of [Au<sub>NP</sub>/G<sub>4</sub>(NH<sup>+</sup>Et<sub>2</sub>Cl<sup>-</sup>)<sub>96</sub>] multilayer films with increasing bilayer number. In Fig. 1(a), one broad peak was observed at around 500–600 nm for [Au<sub>NP</sub>/G<sub>4</sub>(NH<sup>+</sup>Et<sub>2</sub>Cl<sup>-</sup>)<sub>96</sub>] multilayers including Au<sub>NP</sub> with a size of ~3 nm. With increasing bilayer number from 1 to 10, the peak maximum of the SPR band was red-shifted from 520 to 580 nm. For [Au<sub>NP</sub>/G<sub>4</sub>(NH<sup>+</sup>Et<sub>2</sub>Cl<sup>-</sup>)<sub>96</sub>] multilayers containing Au<sub>NP</sub> of ~16 nm size, unlike the spectrum for Au<sub>NP</sub> dispersed in solution, two different peaks were observed in the region of 500–800 nm as shown in Fig. 1(b). The first peak at around 526 nm, attributed to the typical plasmon resonance of isolated Au<sub>NP</sub> similar to that in solution, was maintained without any slight shift during the build-up of multilayers. On the other hand, the other broad peak was significantly red-shifted from 620 to almost 800 nm and simultaneously grown as a dominant peak with increasing bilayer number from 1 to 10 (Fig. 1(b)). The notable growth of the latter band is caused by coupling of surface plasmons occurring from reduced particle–particle distances.<sup>12</sup> With increasing number of bilayers, the amount of Au<sub>NP</sub> adsorbed onto the substrate was increased and spacing between neighboring particles in vertical as well as lateral dimensions was decreased, leading to enhanced collective surface plasmon modes. These phenomena were evidently observed in the SEM images of AuNP-based multilayers films (see ESI,† Fig. S2).

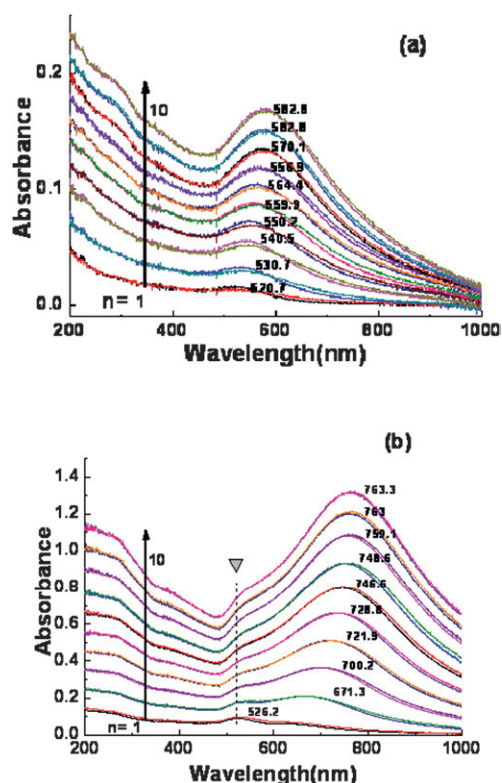


**Fig. 1** UV-vis absorption spectra of [Au<sub>NP</sub>/G<sub>4</sub>(NH<sup>+</sup>Et<sub>2</sub>Cl<sup>-</sup>)<sub>96</sub>]<sub>10</sub> multilayer films containing (a) 3 nm and (b) 16 nm sized Au<sub>NP</sub>. Dipping time in dendrimer solution is 30 min; dipping time in Au<sub>NP</sub> solution is 10 and 30 min for (a) and (b), respectively; pH and concentration of the dendrimer solution are 3.47 and 1 mg/ml (n: number of bilayers).

For quantitative analysis of the adsorbed amounts of Au<sub>NP</sub> and dendrimers during the build-up of Au<sub>NP</sub>/G<sub>4</sub>(NH<sup>+</sup>Et<sub>2</sub>Cl<sup>-</sup>)<sub>96</sub> multilayer films, QCM measurements were conducted with increasing layer number. Fig. 2 shows the frequency changes associated with the adsorbed amount of Au<sub>NP</sub>/G<sub>4</sub>(NH<sup>+</sup>Et<sub>2</sub>Cl<sup>-</sup>)<sub>96</sub> multilayers formed onto the cationic PAH-coated QCM electrodes. By calculating the mass of an Au<sub>NP</sub> with a density of 19.3 g cm<sup>-3</sup>,<sup>13</sup> the average particle number density of 3 and 16 nm-sized Au<sub>NPs</sub> adsorbed per single layer deposition was measured to be  $\sim 6.59 \times 10^{12}$  and  $\sim 1.06 \times 10^{11}$  particles cm<sup>-2</sup>, respectively, from the Sauerbrey equation<sup>14</sup> (Fig. 2).

The frequency changes,  $-\Delta F$ , and the adsorbed mass,  $\Delta m$ , increase regularly with increasing number of Au/G<sub>4</sub>(NH<sup>+</sup>Et<sub>2</sub>Cl<sup>-</sup>)<sub>96</sub> bilayers, indicating that these data are in good agreement with the UV-vis experiments.

### Tuning LSPR properties of the Au<sub>NP</sub>/G<sub>4</sub>(NH<sup>+</sup>Et<sub>2</sub>Cl<sup>-</sup>)<sub>96</sub> multilayer films

In the Au<sub>NP</sub>-containing composite multilayer films, several factors affect the plasmon resonance frequency of the metal such as the size and shape of Au<sub>NP</sub>, the dielectric constant of the surrounding medium and the average distance between adjacent Au<sub>NPs</sub> in lateral and vertical dimensions. Here, we tried to change the inner structure of the multilayer films by removing the dendrimers to modulate the LSPR properties of the films. To this end, the films were exposed to deep UV light with a wavelength

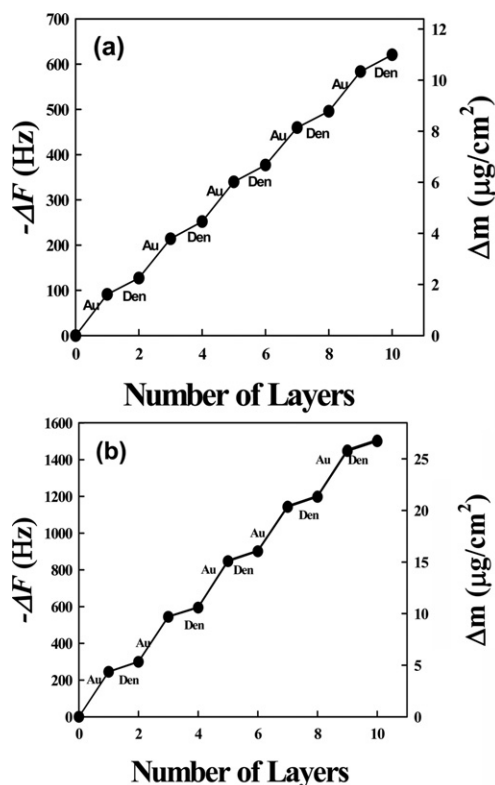


**Fig. 2** Frequency change as a function of the number of bilayers for the assembly of  $[\text{Au}_{\text{NP}}/\text{G}_4(\text{NH}^+\text{Et}_2\text{Cl}^-)]_5$  multilayer films on a QCM electrode. The diameter size of  $\text{Au}_{\text{NPs}}$  was about (a) 3 nm and (b) 16 nm, respectively.

of 254 nm for 24 hours.<sup>15</sup> The morphologies of the initial film and that after UV treatment were investigated and compared by microscopic studies (see ESI,† Fig. S3 and S4). When neighboring  $\text{Au}_{\text{NPs}}$  are brought into proximity (within  $\sim 2.5$  times the particle diameter), the coupled plasmons are red-shifted in a distance-dependent manner.<sup>16</sup> As shown in Fig. 3, a remarkable red-shift of the surface plasmon extinction peak was observed for the UV-irradiated film. In Fig. 3(a) and (b), red-shifts of  $\sim 42.2$  nm and  $\sim 45$  nm were observed for multilayers with  $\sim 3$  nm and  $\sim 16$  nm  $\text{Au}_{\text{NPs}}$ , respectively. This observation was strongly supported by frequency (or mass) changes measured from QCM for the samples before and after UV light irradiation (see ESI,† Fig. S5). Here, it should be noted that the reformation of dendrimers seems not to be complete since the band at 285 nm is still present. This reminds us that UV irradiation allows the fragmentation of the dendrimers with recombination.<sup>17</sup>

As an opposite strategy, the effect of increased spacing of dendrimer layers between  $\text{Au}_{\text{NP}}$  layers on the LSPR properties was investigated through the addition of an ionic salt into the dendrimer deposition solution. Upon the addition of ionic salts into the PE solution,<sup>18</sup> the dimension of PEs expands due to reduced electrostatic repulsion between neighboring same charged species. We added 0.5 M NaCl to the dendrimer solution and fabricated salt-containing Au/dendrimer multilayer films. The perspective views of the films containing NaCl were also investigated by microscopic studies (see ESI,† Fig. S3(c) and S4(c)). Fig. 4 shows the surface plasmon absorption of

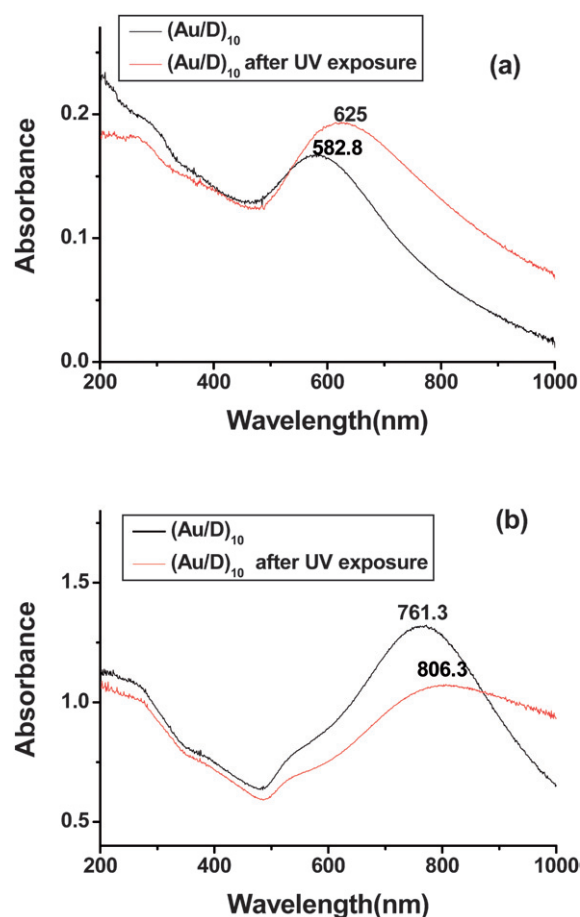


**Fig. 3** UV-vis absorption spectra of  $[\text{Au}_{\text{NP}}/\text{G}_4(\text{NH}^+\text{Et}_2\text{Cl}^-)]_{10}$  multilayer films containing (a) 3 nm and (b) 16 nm  $\text{Au}_{\text{NPs}}$  before and after exposure to deep UV light for 24 hours. The numbers indicate the peak positions of the LSPR bands.

salt-containing  $\text{Au}/\text{G}_4(\text{NH}^+\text{Et}_2\text{Cl}^-)_{96}$  multilayer films with two different sized  $\text{Au}_{\text{NPs}}$ . It can be seen that, for the case of Au composite multilayers with 3 nm size (Fig. 4(a)), a clear peak is observed around 285 nm. As shown in the spectra of Au composite films with 16 nm size (Fig. 4(b)), a similar trend was observed at the same region compared with that of salt-free films in Fig. 1. That is, the band intensity increases regularly with increasing layer number.

However, the degree of red-shift of  $\lambda_{\text{max}}$  wavelength of  $\text{Au}_{\text{NPs}}$  is lower than that of salt-free films at the same layer number. In order to fully understand the changes in the multilayer films, we compared spectra of salt-free and salt-containing films. Fig. 5(a) and (b) show representative spectra from two different samples of salt-free and salt-containing films with 10 bilayers.  $\lambda_{\text{max}}$  wavelength of  $\text{Au}_{\text{NPs}}$  in the original salt-free film is at 582.7 nm, while that of  $\text{Au}_{\text{NPs}}$  in the salt-containing film changes to 554.4 nm. In the case of multilayer with  $\text{Au}_{\text{NPs}}$  of 16 nm size, the same result was observed. *i.e.*,  $\lambda_{\text{max}}$  wavelength of  $\text{Au}_{\text{NPs}}$  blue-shifted from  $\sim 777.6$  nm for the salt-free film to  $\sim 682.2$  nm for the salt-containing film. The results can be interpreted as follows: the dendrimer molecules are swollen upon the addition of salt, leading to an increase of the average distance between Au layers. In the resulting film geometry, the strength of coupling

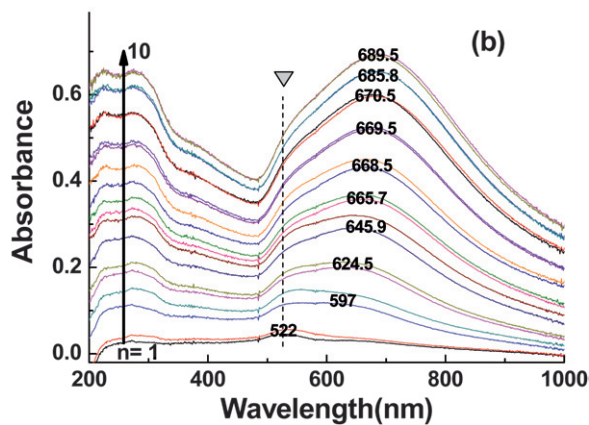
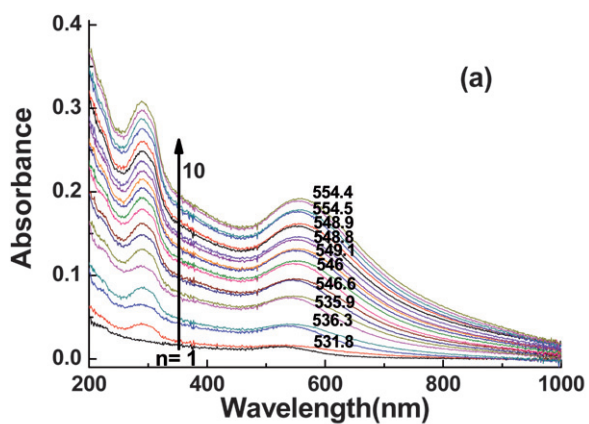


**Fig. 4** UV-vis absorption spectra of  $[\text{Au}_{\text{NP}}/\text{G}_4(\text{NH}^+\text{Et}_2\text{Cl}^-)_{96}]_{10}$  multilayer films in the presence of 0.5 M NaCl solution. The diameter of  $\text{Au}_{\text{NPs}}$  was about (a) 3 nm and (b) 16 nm, respectively; dipping time in dendrimer solution is 30 min and dipping time in Au solution is 10 and 30 min for (a) and (b), respectively ( $n$ : number of bilayers).

between neighboring Au layers weakens. This is reflected as a distinct blue shift of the LSPR band.

#### LSPR sensing properties of the Au films

Among the potential functions that the films may have, we primarily investigated the sensing activity for dielectric environments. Here, we employed five alcohols with different refractive indices ( $n$ ) as model surrounding media. Fig. 6(a) shows absorption spectra of 5 bilayers with 3 nm  $\text{Au}_{\text{NPs}}$ , after removing the dendrimers by UV exposure, followed by immersion in methanol, ethanol, 1-propanol, 1-butanol and 1-pentanol, whose refractive indices are 1.329, 1.361, 1.385, 1.399 and 1.410, respectively. We can observe that the peak maximum of Au multilayer films exhibits a moderate red-shift as the refractive index of the solvents increases in the range of 1.33–1.41. Mie theory predicts a similar red shift in the position of the absorbance peak ( $\lambda_{\text{max}}$ ) consistent with experimental observations.<sup>19</sup> The same experimental protocol was applied to a 10 bilayers film after removing the dendrimers, and one can observe a more distinct red shift (Fig. 6(b)) compared with the case of 5 bilayers. A plot of  $\lambda_{\text{max}}$  vs refractive index is summarized for the two Au films as shown in Fig. 6(c). Linear fits to the data for

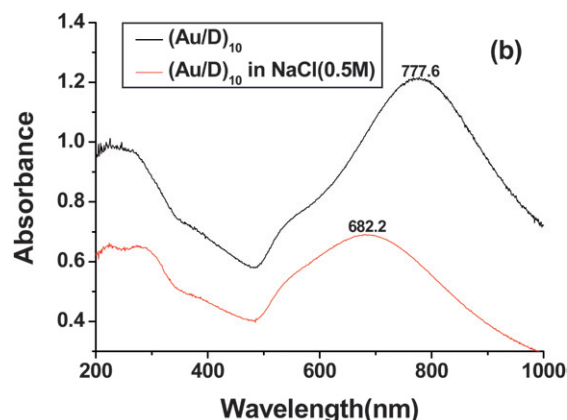
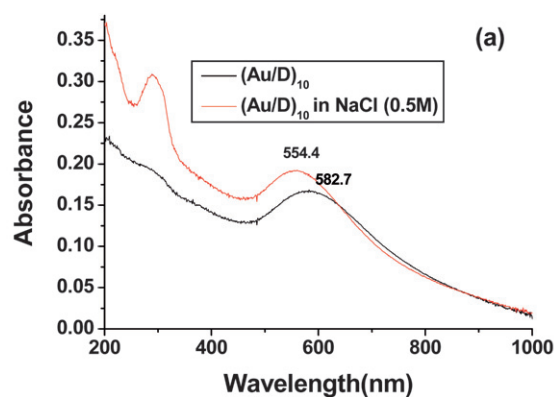


**Fig. 5** UV-vis absorption spectra of  $[\text{Au}_{\text{NP}}/\text{G}_4(\text{NH}^+\text{Et}_2\text{Cl}^-)_{96}]_{10}$  multilayer films with and without 0.5 M NaCl. In this case,  $\text{Au}_{\text{NPs}}$  with (a) 3 nm and (b) 16 nm were used for the build-up of multilayers. The numbers indicate the peak positions of the LSPR bands.

Au films obtained from 5 and 10 bilayers give sensitivity factors of 114.7 and 542 nm/refractive index units (RIU), respectively. The higher sensing capability, which is known to be proportional to the square of the electric field, of the film with more  $\text{Au}_{\text{NPs}}$  is interpreted to originate from its stronger plasmon field that extends from the metal film.<sup>20</sup> We also found that the absorbance curves become broader for the 10 bilayers sample. Thus, within this limited refractive index range (1.33–1.41), it is reasonable to assume a linear response of the sensing. However, for a wider range of refractive indices, a linear fit may not apply. These results clearly show that the optical absorbance of an immobilized multilayer of gold colloids is sensitive to the refractive index of the surrounding bulk medium.

#### Conclusions

In summary, multilayer films composed of Au nanoparticles and dendrimers were fabricated by an electrostatic LbL method. We systematically investigated the LSPR properties of the  $\text{Au}_{\text{NPs}}$  in multilayers with different sizes of  $\text{Au}_{\text{NP}}$  and varying the particle–particle distance through ionic strength control and UV irradiation. The observed optical phenomena could be explained reasonably by the theory of near-field interparticle coupling. The Au films after removing dendrimers by UV exposure show

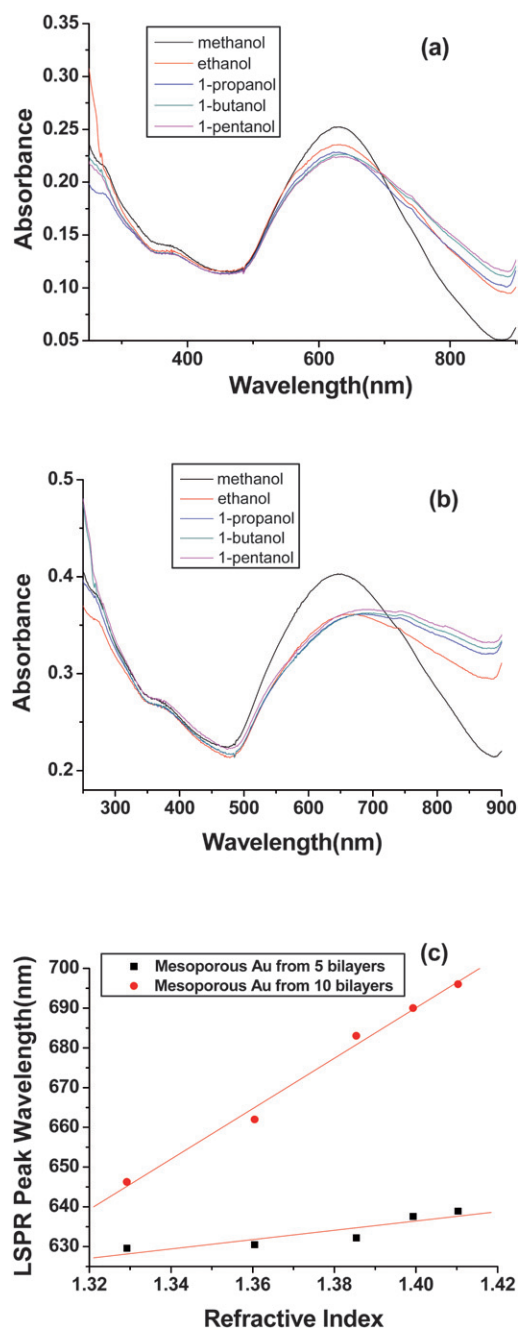


**Fig. 6** UV-vis absorption spectra of (a)  $[\text{Au}_{\text{NP}}/\text{G}_4(\text{NH}^+\text{Et}_2\text{Cl}^-)_{96}]_5$  and (b)  $[\text{Au}_{\text{NP}}/\text{G}_4(\text{NH}^+\text{Et}_2\text{Cl}^-)_{96}]_{10}$  multilayer films with 3 nm  $\text{Au}_{\text{NPs}}$  after UV exposure followed by immersion in alcohols with different refractive indices. (c) Plot of the LSPR peak wavelength as a function of refractive index of alcohols for mesoporous Au obtained from 5 (■) and 10 (●) bilayers containing 3 nm  $\text{Au}_{\text{NPs}}$ .

a red-shift, while salt-containing hybrid films exhibit a blue-shift as a result of the change of average distance between Au layers. These results evidently imply that the LSPR properties of Au-containing multilayer films can be tuned by controlling the strength of LSPR coupling between neighboring  $\text{Au}_{\text{NPs}}$  in lateral and vertical dimensions. Furthermore, we also demonstrated that such Au-containing multilayer films have a reasonably good sensing response for the refractive index change of the

surrounding medium. The experimental protocol and results derived from this study can be exploited to design and fabricate highly sensitive optical biosensor devices.

## Acknowledgements

This work was supported by the Korea Science and Engineering Foundation (KOSEF) grant funded by the Korea government (MEST) (No. R11-2005-008-00000-0 and R01-2008-000-11712-0 for D. H. Kim; R01-2008-000-10551-0 and R11-2005-048-00000-0 for J. Cho) and by the Research Program 2008 of Kookmin University in Korea.

## References

- (a) W. L. Shi, H. Zeng, Y. Sahoo, T. Y. Ohulchanskyy, Y. Ding, Z. L. Wang, M. Swihart and P. N. Prasad, *Nano Lett.*, 2006, **6**, 875; (b) H. Yu, M. Chen, P. M. Rice, S. X. Wang, R. L. White and S. H. Sun, *Nano Lett.*, 2005, **5**, 379.
- (a) X. H. Lou, C. Y. Wang and L. He, *Biomacromolecules*, 2007, **8**, 1385; (b) J. Chen, F. Saeki, B. Wiley, H. Cang, M. J. Cobb, Z. Li, L. Au, H. Zhang, M. J. Kimmey, X. Li and Y. Xia, *Nano Lett.*, 2005, **5**, 473.
- N. T. K. Thanh, A. Vernhet and Z. Rosenzweig, *Springer Ser. Chem. Sens. Biosens.*, 2005, **3**, 261.
- (a) M. C. Daniel and D. Astruc, *Chem. Rev.*, 2004, **104**, 293; (b) J. Shan, M. Nuopponen, H. Jiang, T. Viitala, E. Kauppinen, K. Kontturi and H. Tenhu, *Macromolecules*, 2005, **38**, 2918; (c) A. E. Saunders, I. Popov and U. Banin, *J. Phys. Chem. B*, 2006, **110**, 25421.
- (a) E. Granot, E. Katz, B. Basnar and I. Willner, *Chem. Mater.*, 2005, **17**, 4600; (b) S. J. Guo, Y. X. Fang, S. J. Dong and E. Wang, *J. Phys. Chem. C*, 2007, **111**, 17104.
- (a) E. Hutter and J. H. Fendler, *Adv. Mater.*, 2004, **16**, 1685; (b) A. Moores and F. Goettmann, *New J. Chem.*, 2006, **30**, 1121.
- (a) C. J. Murphy, T. K. Sau, A. M. Gole, C. J. Orendorff, J. X. Gao, L. F. Gou, S. E. Hunyadi and T. Li, *J. Phys. Chem. B*, 2005, **109**, 13857; (b) M. M. Miller and A. A. Lazarides, *J. Phys. Chem. B*, 2005, **109**, 21556; (c) C. Noguez, *J. Phys. Chem. C*, 2007, **111**, 3806; (d) K. L. Kelly, E. Coronado, L. L. Zhao and G. C. Schatz, *J. Phys. Chem. B*, 2003, **107**, 668; (e) S. Eustis and M. A. El-Sayed, *Chem. Soc. Rev.*, 2006, **35**, 209.
- (a) S. K. Ghosh and T. Pal, *Chem. Rev.*, 2007, **107**, 4797; (b) P. K. Jain, W. Y. Huang and M. A. El-Sayed, *Nano Lett.*, 2007, **7**, 2080; (c) P. K. Jain and M. A. El-Sayed, *J. Phys. Chem. C*, 2008, **112**, 4954; (d) C. L. Haynes, A. D. McFarland, L. L. Zhao, R. P. Van Duyne, G. C. Schatz, L. Gunnarsson, J. Prikulis, B. Kasemo and M. Kall, *J. Phys. Chem. B*, 2003, **107**, 7337; (e) E. M. Hicks, S. L. Zou, G. C. Schatz, K. G. Spears, R. P. Van Duyne, L. Gunnarsson, T. Rindzevicius, B. Kasemo and M. Kall, *Nano Lett.*, 2005, **5**, 1065; (f) V. V. Agrawal, N. Varghese, G. U. Kulkarni and C. N. R. Rao, *Langmuir*, 2008, **24**, 2494.
- (a) J. Cho and F. Caruso, *Chem. Mater.*, 2005, **17**, 4547; (b) G. Q. Jiang, A. Baba, H. Ikarashi, R. S. Xu, J. Locklin, K. R. Kashif, K. Shinbo, K. Kato, F. Kaneko and R. Advincula, *J. Phys. Chem. C*, 2007, **111**, 18687; (c) N. Malikova, I. P. Santos, M. Schierhorn, N. A. Kotov and L. M. Liz-Marzán, *Langmuir*, 2002, **18**, 3694; (d) Q. Wang, X. H. Yang and K. M. Wang, *Sensors and Actuators B*, 2007, **123**, 227; (e) K.-K. Chia, R. E. Cohen and M. F. Rubner, *Chem. Mater.*, 2008, **20**, 6756; (f) B. M. Budhlall, M. Marquez and O. D. Velev, *Langmuir*, 2008, **24**, 11959; (g) H. Kawasaki, T. Sugitani, T. Watanabe, T. Yonezawa, H. Moriwaki and R. Arakawa, *Anal. Chem.*, 2008, **80**, 7524; (h) K. V. Sarathy, P. J. Thomas, G. U. Kulkarni and C. N. R. Rao, *J. Phys. Chem. B*, 1999, **103**, 399.
- (a) K. C. Grabar, R. G. Freeman, M. B. Hommer and M. J. Natan, *Anal. Chem.*, 1995, **67**, 735; (b) N. R. Jana, L. Gearheart and C. J. Murphy, *Adv. Mater.*, 2001, **13**, 1389.
- (a) N. Launay, A.-M. Caminade, R. Lahana and J. P. Majoral, *Angew. Chem., Int. Ed. Engl.*, 1994, **33**, 1589; (b) C. Loup, M. A. Zanta, A.-M. Caminade, J. P. Majoral and B. Meunier,

- 
- Chem. Eur. J.*, 1999, **5**, 3644; (c) N. Launay, A.-M. Caminade and J. P. Majoral, *J. Organomet Chem.*, 1997, **529**, 51; (d) M. Slany, A.-M. Caminade and J. P. Majoral, *Tetrahedron Lett.*, 1996, **37**, 9053.
- 12 K. C. Grabar, R. G. Freeman, M. B. Hommer and M. J. Natan, *Anal. Chem.*, 1995, **67**, 735.
- 13 J. S. Lee, J. Cho, C. Lee, I. Kim, J. J. Park, Y. M. Kim, H. J. Shin, J. Lee and F. Caruso, *Nature Nanotechnology*, 2007, **2**, 790.
- 14 G. Z. Sauerbery, *Phys.*, 1959, **155**, 206.
- 15 D. H. Kim, O.-J. Lee, E. Barriau, X. Li, A.-M. Caminade, J.-P. Majoral, H. Frey and W. Knoll, *J. Nanosci. Nanotechnol.*, 2006, **6**, 3871.
- 16 B. M. Reinhard, M. Siu, H. Agarwal, A. P. Alivisatos and J. Liphardt, *Nano Lett.*, 2005, **5**, 2246.
- 17 J. C. Blais, C. O. Turrin, A.-M. Caminade and J. P. Majoral, *Anal. Chem.*, 2000, **72**, 5097.
- 18 O. V. Lebedeva, B. S. Kim, K. Vasilev and O. I. Vinogradova, *J. Colloid Interface Sci.*, 2005, **284**, 455.
- 19 A. C. Templeton, J. J. Pietron, R. W. Murray and P. Mulvaney, *J. Phys. Chem. B*, 2000, **104**, 564.
- 20 (a) L. S. Jung, C. T. Campbell, T. M. Chinowsky, M. N. Mar and S. S. Yee, *Langmuir*, 1998, **14**, 5636; (b) A. J. Haes, S. Zou, G. C. Schatz and R. P. Van Duyne, *J. Phys. Chem. B*, 2004, **108**, 109.